ELSEVIER

Chemical Engineering Journal 84 (2001) 355–366

Chemical Engineering Journal

www.elsevier.com/locate/cej

A capacity model for vertical pipes and packed columns based on entrainment

Geert F. Woerlee*, Joop Berends

Laboratory for Process Equipment, Delft University of Technology, Leeghwaterstraat 44, NL-2628 CA Delft, The Netherlands

Received 4 January 1999; received in revised form 4 December 2000; accepted 4 December 2000

Abstract

This study bridges flooding correlations in vertical pipes and packed towers. It is shown that the frictional forces of the gas on the liquid interface can either directly carry the liquid film upwards or induce droplet formation and, therefore, entrainment of the gas phase. A model is presented that estimates the entrainment flood point. The model does not fully explain the flooding phenomena. However, as is shown in this study, a total flooding explanation cannot be expected from any theory. Nevertheless, the model provides an estimation method that describes the relative changes of flood point with the physical properties and the geometry. This is accomplished by taking into account the lift force on entrained droplet. It is possible to estimate the flood point as function of the viscosity, density, surface tension, and the geometry of the packing.

Keywords: Flooding; Entrainment; Vertical tubes; Packed columns

1. Introduction

Liquid flow reversal or flooding in counter-current falling film operations has been a subject of experimental and analytical study for over half a century. Perhaps the most common counter-current flow situation where flooding is important is in packed towers. Despite many research activities, there are still uncertainties on various aspects concerning the influences on the flood point, e.g. equipment size, gas inlet and outlet configurations, operating conditions, and physical properties of the system. This is caused by the fact that the physical mechanisms governing the process of flooding are not completely understood even for the simplest geometry, a vertical pipe. This study intends to bridge flooding correlations in vertical pipes and the correlations for packed towers. Although, it will not be possible to address all difficulties related to the flooding mechanism, some influences concerning physical properties and geometry will be elucidated, by applying data analysis and theoretical considerations.

Flooding is induced by the frictional forces of the gas phase on the liquid phase. [1], postulated that at least two types of liquid-flow instability can occur to initiate flooding. The first type, observed in conventional random packing and geometries with a small specific interface area, is due to the interaction between the liquid hold-up and pressure gradient. The pressure gradient and the forces on the liquid film are such that the whole film starts to flow up-wards. This macroscopic flooding was discussed in an earlier paper [2,3] refers to the macroscopic flooding mechanism as the system limit. The second type of flooding is entrainment flooding. The frictional forces cause waves on the interface. These waves become unstable and droplets are formed which are carried up-ward with the gas. The wave instabilities are considered as the most plausible cause for flooding [4]. However, they do not explain various aspects of packing behaviour, i.e. the influence of the inclination angle of the packing surface, the relative insensitivity of the flood point for surface tension, etc. Although, the wave instability approach can predict a point at which droplets can be created, this does not necessarily mean that they are created. The instability requires a certain pipe length, or residence time, to build-up. Besides, when most droplets are deposited on the falling film, the condition at which droplets are generated, does not mark the flood point. An engineer would like to know the point at which liquid is carried up against gravity with the gas flow. It is for this reason that in the presented paper the definition of flooding as defined by [5] is applied, flooding is the moment, when the whole liquid flow is disrupted and expelled from the top of the equipment.

The capacity of a packed column is not directly related to the mass transfer, but the flood point determines the upper

* Corresponding author. Present address: FeyeCon Development & Implementation, Javakade 192, NL-1019 RW, Amsterdam.
Tel.: +31-20-419-6050; fax: +31-20-419-6051.
E-mail address: geert@feyecon.com (G.F. Woerlee).

1385-8947/01/$ – see front matter
PII: S1385-8947(01)00127-9

Nomenclature

a_p	specific packing area $a_p = 2\epsilon_0/r_0$ (m^2/m^3)
Bo	bond number $Bo = 2r_{int}^2 g(\rho_G - \rho_L)/\sigma$
C	constant in Wallis correlation
C_{cor}	correction factor for physical properties
C_G	capacity factor (m/s)
C_G^{crit}	critical capacity factor (m/s)
$C_{G,meas}^{crit}$	measured critical capacity factor (m/s)
$C_{G,model}^{crit}$	critical capacity factor calculated with the model (m/s)
C_r	relative capacity factor
C_t	on position dependent parameter of the lift force
d_e	entrained drop diameter (m)
d_{max}	maximum stable drop diameter (m)
D_{col}	column diameter (m)
f	smooth pipe friction factor
f_p	friction factor of the packing
F_l	lift force on entrained droplet (N)
F_d	drag force on entrained droplet (N)
F_g	gravitational force on entrained droplet (N)
g	gravitational acceleration (m/s^2)
G''	gas load ($kg/s/m^2$)
Ga_p	packing Galileo number $Ga_p = 4\,\Delta\rho\,\rho_L g \cos\alpha/3\,\eta_L^2 a_p^3$
h	liquid film thickness (m)
h_L	liquid hold-up (m^3/m^3)
H_{col}	column height (m)
K_G	gas Kutateladze number $K_G = u_{SG}\left(\rho_G^2/g\,\sigma(\rho_G - \rho_L)\right)^{0.25}$
L''	liquid load ($kg/s/m^2$)
m	constant in Wallis correlation
m_1	power constant for surface tension correction
m_2	power constant for liquid viscosity correction
$p_{1,2}$	pressure (Pa)
$\partial p/\partial z$	pressure drop over equipment (Pa/m)
$\partial p_f/\partial z$	frictional pressure drop (Pa/m)
r	radial co-ordinate
r_0	hydraulic radius $r_0 = 2\epsilon_0/a_p$ (m)
r_{int}	interface radius ($r_{int} = \theta r_0$) (m)
Re_G	gas phase Reynolds number $Re_G = \rho_G((u_{SG}/\theta^2\varepsilon_0\cos\alpha) - u_{int})2\,\theta r_0/\eta_G$
Re_L	liquid phase Reynolds number $Re_L = 4\,\rho_L u_{SL}/\eta_L a_p$
u_d	drop velocity (m/s)
u_{int}	interface velocity (m/s)
u_G	gas velocity (m/s)
u_{SG}	superficial gas velocity (m/s)
u_{SG}^{crit}	critical superficial gas velocity (m/s)
u_{SL}	superficial liquid velocity (m/s)
U_G^*	dimensionless superficial gas velocity
U_L^*	dimensionless superficial liquid velocity
$\bar{v}$	velocity of turbulent eddies (m/s)
$We_{crit\text{-}1}$	critical Weber number $We_{crit\text{-}1} = \rho_G((u_{SG}/\varepsilon_0\theta^2\cos\alpha) - u_{int})^2 d_{max}/\sigma$
$We_{crit\text{-}2}$	critical Weber number $We_{crit\text{-}2} = 3\,\rho_G(\varepsilon d_{max})^{2/3} d_{max}/\sigma$

Greek letters

α	effective inclination angle (°)
$\Delta\rho$	density difference (kg/m^3)
ϵ	dissipated kinetic energy (m^2/s^3)
ϵ_0	void fraction (m^3/m^3)
γ_1	general turbulence constant ($\gamma_1 = 1.8$)
η_G	dynamic gas viscosity (Pa s)
η_L	dynamic liquid viscosity (Pa s)
θ	relative interface position $\theta = r_{int}/r_0$
Φ	flow parameter
ρ_G	gas density (kg/m^3)
ρ_L	liquid density (kg/m^3)
σ	surface tension (N/m)
ψ_{G-L}	gas–liquid interaction parameter

limit for good inter-phase mass transfer in a counter-current column. Therefore, it is of crucial importance for the column designer to know precisely the capacity limits of a given case. Here, a model is developed to predict flooding in packed columns, which is initiated by entrainment.

2. General flooding considerations

The vertical pipe geometry is a starting point to investigate flooding in more complex geometries. The work of [6] and a recent experimental study of [7] showed the dependence of the flood point in vertical pipes on inlet and outlet geometry, pipe length and gas entrance. These studies showed that the onset of flooding in a vertical pipe is very sensitive to the test-section geometry. Flooding data obtained in vertical pipes is often correlated using the Wallis type equation (see, e.g. [8]):

$$U_G^* + m\sqrt{U_L^*} = C. \tag{1}$$

Here, m and C are dimensionless constants and the dimensionless superficial velocities are related to the superficial gas velocity u_{SG} as

$$U_G^* = u_{SG}\left(\frac{\rho_G}{2r_0 g(\rho_L - \rho_G)}\right)^{0.5}, \tag{1a}$$

and the superficial liquid velocity u_{SL} as

$$U_L^* = u_{SL}\left(\frac{\rho_L}{2r_0 g(\rho_L - \rho_G)}\right)^{0.5}. \tag{1b}$$

Here, r_0 represents the radius of the tube. The basic form of Eq. (1) also is applied for liquid–liquid extraction correlations (see, e.g. [9,10]). The capacity in counter-current

equipment is usually showed as function of the flow parameter (Φ), which is defined as

$$\Phi = \frac{U_L^*}{U_G^*} = \frac{u_{SL}}{u_{SG}}\sqrt{\frac{\rho_L}{\rho_G}}. \quad (2)$$

By isolating the dimensionless gas velocity of Eq. (1),

$$U_G^* = \frac{C^2}{(a + m\sqrt{\Phi})^2}, \quad (3)$$

and by multiplication with the root of the product of the pipe diameter and the gravitational constant, the relation that generally is used for packed columns is found:

$$C_G = u_{SG}\sqrt{\frac{\rho_G}{\rho_L - \rho_G}} = \sqrt{2r_0 g}\,\frac{C^2}{(a + m\sqrt{\Phi})^2}. \quad (4)$$

Here, C_G represents the gas capacity factor. Fig. 1 shows experimental flood points expressed as dimensionless gas velocities as function of the dimensionless liquid velocity for vertical tubes and packing structures. For the packing structures the hydraulic radius $r_0 = 2\epsilon_0/a_p$ is applied, where a_p represents the specific surface area of the packing and ϵ_0 represents the void fraction.

Fig. 1 shows the large difference between the capacity limits of the two vertical pipe configurations. Especially the square-edged bottom configuration causes a local increase of the liquid hold-up that promotes the flooding phenomenon [6,7]. The data show the sensitivity of flooding for subtle aspects of the flow configuration. It is likely that packed beds are sensitive to aspects as gas inlet and packing arrangement as well.

Several authors have attempted to justify the success of Eq. (1), but its general shape is still not completely understood. The most successful theoretical models describing the flooding mechanism in vertical tubes are based on the frictional forces on each phase (see [11]. However, given that liquid–liquid application can be written also in the form of Eq. (1), the latter indicates that an approach based on droplet entrainment could also be effective. When taking the view-point of liquid–liquid applications, for gas–liquid application the dispersed phase is formed by the entrained liquid droplets, while the continuous gas phase should be taken relative towards the interface velocity.

3. The forces on the droplets

Although, under some conditions the friction of the gas with the liquid itself can cause enough upward force to prevent the liquid from flowing down (see, [2]), we believe that the onset of flooding is in most cases due to entrainment of droplets in the gaseous phase. Five entrainment mechanisms are distinguished that could create droplets in a vertical pipe [12], i.e. roll wave shear off, wave undercut [13], bubble burst, liquid impingement, and liquid bulge disintegration. Some of these mechanisms are not possible with thin films. Besides this, the structure of a packed bed will create droplets as well (see, e.g. [14]). In this study it is assumed that due to a mechanism that we will not address, droplets will enter the gas phase. Fig. 2 illustrates that a droplet in the gaseous phase is exposed to three forces. These are the gravitational force F_g, the drag force F_d, and the rotational or lift force F_l. In most present theories, only the gravitational and drag force are used to describe the flooding.

The lift force on the droplets is caused by the velocity gradient of the gas phase and is always directed towards the

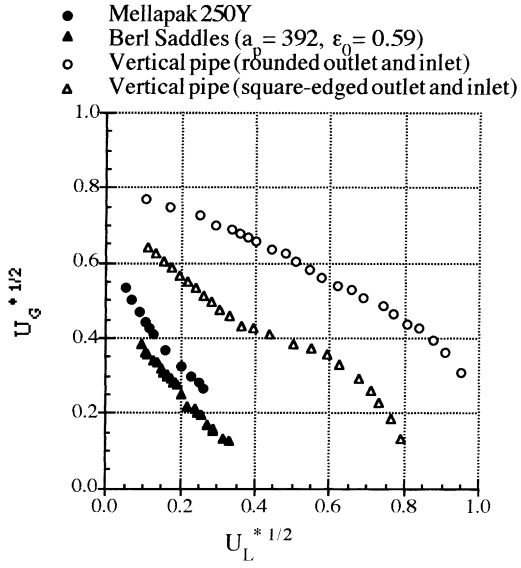

Fig. 1. Maximum square root of the dimensionless superficial gas velocity as function of the square root of the dimensionless superficial liquid velocity, in a vertical one meter tube [7], structured packing [29] and random packing [37].

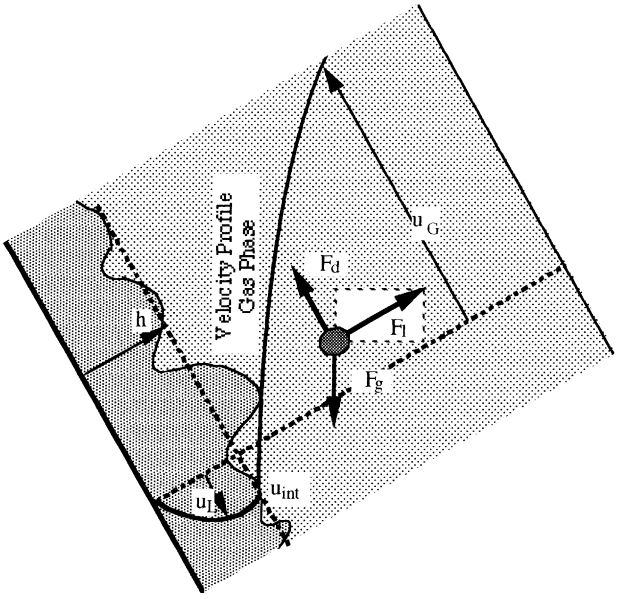

Fig. 2. The three forces on the liquid film. Showing the lift force, the gravitational force and the drag force.

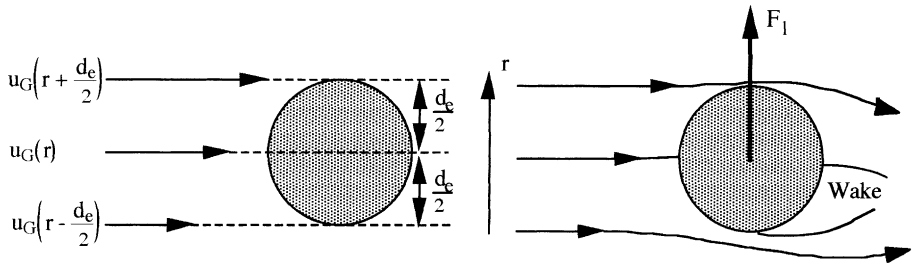

Fig. 3. A droplet in a gradient velocity field (left hand side) and the by this field caused flow pattern and force on the droplet (right hand side).

centre of the tube. The lift force as drawn in Fig. 2 has a component opposite to gravity. However, the droplets created in the upper half of the cross section have a net component directed along with gravity. In case droplets created at the bottom part of the gas flow, they will be exposed to a lift force which has an upwards directed component. This means that the droplets created at the bottom of the channel will be the first which will cause entrainment. For an ideal fluid the lift force can be calculated by determining the rotation over the droplet (see, e.g. [15–17]. For real fluids the phenomenon is more complex and related to the formation of an asymmetric wake at one side of the droplet as shown in Fig. 3 (see, e.g. [18]). We will not attempt to describe the full lift phenomenon, but apply a simple method to quantify its size. With Bernoulli's relation a balance over an entrained droplet is given by (see Fig. 3):

$$p_1 + \tfrac{1}{2}\rho_G u_G^2 \Big| r - \tfrac{d_e}{2} = p_2 + \tfrac{1}{2}\rho_G u_G^2 \Big| r + \tfrac{d_e}{2}, \tag{5}$$

from the pressure difference resulting over the droplet the lift force can be approximated as

$$\begin{aligned} &\tfrac{1}{2}\rho_G\left(u_G(r) - u'(r)\tfrac{1}{2}d_e\right)^2 - \tfrac{1}{2}\rho_G\left(u_G(r) - u'(r)\tfrac{1}{2}d_e\right)^2 \\ &\quad = p_2 - p_1, \\ &\rho_G u_G(r)u'(r)d_e = \frac{F_l}{(\pi/4)d_e^2} \Rightarrow F_l = \tfrac{1}{4}\pi\,\rho_G u_G(r)u'(r)d_e^3. \end{aligned} \tag{6}$$

Here, the $u_G(r)$ represents the velocity of the gas compared with the velocity of the droplet. Due to the product of the local velocity and the gradient of the velocity the force will have a maximum. To approximate the product of the local velocity and the gradient of the local velocity in a turbulent flow, the universal velocity profile correlation of [19] is applied. Using the universal profile, the force in the bottom of the tube is rewritten as

$$F_l = \rho_G \tfrac{1}{4}\pi d_e^3 \left(\frac{u_{SG}}{\varepsilon_0\,\theta^2\cos\alpha} - u_{int}\right)\frac{C_t}{r_{int}} \times \left(\frac{u_{SG}}{\varepsilon_0\theta^2\cos\alpha} - u_d\right), \tag{7}$$

where C_t represents a dimensionless parameter. This parameter depends on the relative position in the gas flow and the gas Reynolds number. Fig. 4 shows the dependence of the coefficient on the Reynolds number and radial position. Given the gas Reynolds numbers normally applied in a packed bed the value of the maximum value of the parameter C_t will be in the range of 3–6. In Eq. (7), u_d represents the droplet velocity and u_{int} the interface velocity, these velocity are normally downwards and, therefore have a negative sign. The normalised interface position ($\theta = r_{int}/r_0$) is used to express the liquid hold-up ($\epsilon_0\theta^2$), while the cosine term corrects the velocity for the flow angle.

The drag force can be expressed in a number of ways, which are related to the type of flow and the droplet size. A constant friction factor of 0.44 can be applied for particles

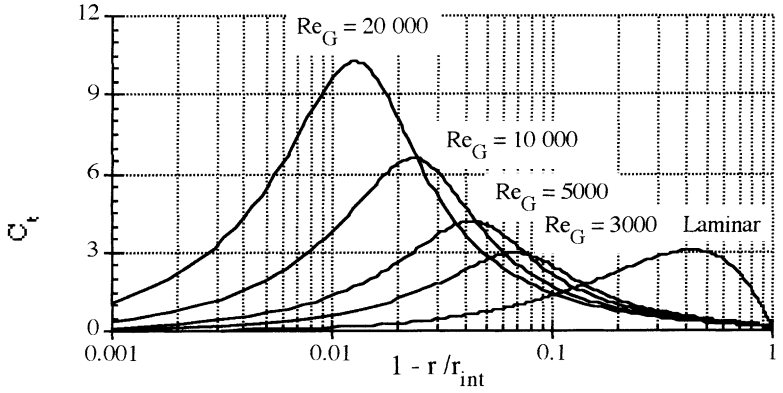

Fig. 4. The coefficient as defined in Eq. (7) for zero droplet and interface velocity as function of the dimensionless radius and the Reynolds number.

in a turbulent stream (see, e.g. [18,20]), such that the drag force F_d on an entrained droplet can be expressed as

$$F_d = 0.055\,\pi d_e^2\,\rho_G \left|\frac{u_{SG}}{\varepsilon_0\,\theta^2\cos\alpha} - u_d\right| \times \left(\frac{u_{SG}}{\varepsilon_0\,\theta^2\cos\alpha} - u_d\right). \quad (8)$$

Taking the pressure drop into account the gravitational force can be written as

$$F_g = \tfrac{1}{6}\,\pi d_e^3 \left(\rho_L - \rho_G + \frac{1}{g}\frac{\partial p}{\partial z}\right) g. \quad (9)$$

When the gas flow is upwards, the pressure drop is negative, so that in that case the effective gravitational force decreases. Taking the gas flows at an inclination angle α, the forces balance in the direction along with gravity reads:

$$F_d\cos\alpha + F_l\sin\alpha = F_g. \quad (10)$$

The boundary condition for flooding is defined as a critical gas velocity at which the velocity of the droplet becomes zero (u_{SG}^{crit}; $u_d = 0$). Eq. (10) can be rewritten using this condition so that the balance reads:

$$\left(\frac{u_{SG}^{crit}}{\varepsilon_0\,\theta^2\cos\alpha}\right)^2 \frac{\cos\alpha}{d_e} + \frac{C_t}{0.22}\left(\frac{u_{SG}^{crit}}{\varepsilon_0\,\theta^2\cos\alpha} - u_{int}\right)\left(\frac{u_{SG}^{crit}}{\varepsilon_0\,\theta^2\cos\alpha}\right)\frac{\sin\alpha}{r_{int}} = 3\,g\left(\frac{\rho_L - \rho_G(1/g)(\partial p/\partial z)}{\rho_G}\right). \quad (11a)$$

Substitution of an average coefficient as ($\bar{C}_t = 1.75$), this results in

$$\rho_G\left(\frac{u_{SG}^{crit}}{\varepsilon_0\,\theta^2\cos\alpha}\right)^2\left(\frac{\cos\alpha}{d_e} + \frac{8\sin\alpha}{r_{int}}\left(1 - \frac{u_{int}\,\varepsilon_0\,\theta^2\cos\alpha}{u_{SG}}\right)\right) = 3\left(\rho_L - \rho_G + \frac{1}{g}\frac{\partial p}{\partial z}\right) g. \quad (11b)$$

This average value agrees with the lower cross section part of the gas channel. Given the rough approach of the presented model a more accurate determination of the coefficient (C_t) cannot be justified. By neglecting the interface velocity the critical capacity factor is isolated as

$$C_G^{crit} = u_{SG}^{crit}\sqrt{\frac{\rho_G}{\rho_L - \rho_G}} = \varepsilon_0\,\theta^2\cos\alpha\sqrt{\frac{3\,g}{(\cos\alpha/d_e) + (4a_p/\varepsilon_0\,\theta)\sin\alpha}} \times\sqrt{\frac{\rho_L - \rho_G + (1/g)(\partial p/\partial z)}{\rho_L - \rho_G}}. \quad (12)$$

4. The droplet size

The capacity factor relation (12) includes a characteristic droplet diameter. Several approaches can be applied to determine a droplet diameter. Again much will depend on the view one has on how the droplets are formed. However, it is assumed that the droplets have entered the gas phase and, therefore, the gas phase behaviour will determine the size of the droplets. In a packing the mechanisms for droplet break-up could either be caused by velocity gradients or by the turbulence of the flow. Both mechanisms were discussed by [21]. When it is assumed that the drop size is determined by the velocity gradients, a critical Weber number related to the maximum stable drop diameter d_{max} is used:

$$We_{crit\text{-}2} = \frac{\rho_G((u_{SG}/\varepsilon_0\,\theta^2\cos\alpha) - u_{int})^2 d_{max}}{\sigma}. \quad (13)$$

In most applications, a typical critical Weber numbers of 10–22 is found [12,21,22].

The second mechanism for droplet break-up is caused by the turbulent flow. Assuming isotropic homogeneous turbulence, the average velocity of the eddies ($\bar{v}$) on the scale of the droplet can be obtained by integrating the general Kolmogorov energy distribution law up to the maximum size of the droplets (see, e.g. [23]) as

$$\bar{v}^2 = \int_{d_{max}^{-1}}^{\infty} \gamma_1\,\varepsilon^{2/3}k^{-5/3}\,dk = \tfrac{3}{2}\,\gamma_1(\varepsilon d_{max})^{2/3} = 3(\varepsilon d_{max})^{2/3}. \quad (14)$$

In this equation, ϵ represents the dissipated energy and γ_1 the general turbulence constant, which is taken equal to 2. [21,24] used this average velocity to obtain a critical Weber number:

$$We_{crit\text{-}2} = \frac{\rho_G\bar{v}^2 d_{max}}{\sigma} = 3\,\frac{\rho_G(\varepsilon d_{max})^{2/3}d_{max}}{\sigma}. \quad (15)$$

Applying experimental data he found a critical Weber number that was a little larger than unity for the maximum stable droplet. The sizes of the droplets are distributed and the maximum stable droplet size needs to be connected with an effective entrained droplet size. Here, an effective entrained droplet diameter (d_e) is taken as one fourth of the maximum entrained droplet calculated with Eq. (15). The effective entrained droplet is expressed as

$$d_e = \tfrac{1}{4}d_{max} = \frac{0.725}{4}\left(\frac{\sigma}{\rho_G}\right)^{0.6}\varepsilon^{-0.4} = \frac{0.725}{4} \times\left(\frac{\sigma}{\rho_G}\right)^{0.6}\left(-\frac{(\partial p/\partial z)((u_{SG}/\varepsilon_0\,\theta^2) - u_{int}\cos\alpha)}{\rho_G}\right)^{-0.4} = \frac{0.725}{4}\left(\frac{\sigma}{\rho_G}\right)^{0.6} \times\left(\frac{\theta r_0}{f_p(1+\psi_{G\text{–}L})|(u_{SG}/\varepsilon_0\,\theta^2) - u_{int}\cos\alpha|^3}\right)^{0.4} \quad (16)$$

Expression (16) determines the entrained droplet size in Eq. (12). The choice of 1/4 of the maximum droplet diameter is not crucial, but it appears a logical selection (see, e.g. [25]). Besides, it is in accordance with the flooding relation in a vertical pipe. A general relation for the total dissipated kinetic energy in the gas phase is found by using the pressure drop over the geometry. The packing friction factor (f_p) is determined using dry-pressure drop measurements and the gas–liquid interaction parameter (ψ_{G-L}) is expressed as (see [2]):

$$\psi_{G-L} = \sinh\left[\frac{34\times10^{-15}(1-\theta^2)^7}{(\cos\alpha)^9 Re_L^2 Ga_p^{-2}} Re_L Re_G^{1.5}\frac{\rho_L\,\eta_L}{\rho_G\,\eta_G}\right], \tag{17}$$

where Ga_p is the packing Galileo number. The gas–liquid interaction parameter only becomes noticeable when both the gas and liquid flows are substantial.

5. Results and discussion

Eq. (16) can be used in combination with Eq. (12), so that the critical capacity factor can be written as

$$C_G^{crit} = \left(\frac{3(\varepsilon_0\,\theta^2\cos\alpha)^2(g+[1/(\rho_L-\rho_G)](\partial p/\partial z))}{(4/0.725)[f_p a_p(1+\psi_{G-L})|(u_{SG}^{crit}/\varepsilon_0\,\theta^2)-u_{int}\cos\alpha|^3/2\,\theta\,\varepsilon_0]^{0.4}(\rho_G/\sigma)^{0.6}\cos\alpha+(4a_p/\theta\,\varepsilon_0)\sin\alpha}\right)^{0.5}. \tag{18}$$

Unfortunately, it cannot be justified to neglect terms in general, so that it is not possible to obtain an explicit expression for the critical capacity factor. However, given the physical properties of the system and the liquid flow the critical superficial gas velocity simply is solved by iteration. The macroscopic properties regarding the frictional and total pressure drops ($\partial p_f/\partial z$), ($\partial p/\partial z$), the interface velocity (u_{int}), the relative interface position (θ) and macroscopic flooding, are solved with the model presented in our earlier study [2].

5.1. Vertical pipe geometry

When Eq. (18) is used for a vertical pipe the equation simplifies as

$$C_G^{crit} = 0.737\,\theta^2\left(\frac{\sigma}{\rho_G}\right)^{0.3} \times\left(\frac{\theta r_0}{f(1+\psi_{G-L})|(u_{SG}^{crit}/\theta^2)-u_{int}|^3}\right)^{0.2} \times\left(g+\frac{1}{(\rho_L-\rho_L)}\frac{\partial p}{\partial z}\right)^{0.5}, \tag{19}$$

where the packing friction factor is replaced by the friction factor of a smooth pipe. Fig. 5 shows measured and estimated flood points over the full liquid flow range. Here, two measured geometries [7] are compared with the estimated curve of Eq. (19).

Firstly, it is noticed that the estimation is for a pipe with rounded inlet and outlet. This is not surprising since the model uses idealised flow conditions and the square edged configuration causes an additional liquid hold-up due to contraction of the gas flow. Secondly, as indicated in the graph a relative smooth transition to macroscopic flooding is found. The liquid film can no longer flow downwards due to the frictional forces and the pressure drop over the internals.

For thin films, the interface velocity, the pressure drop and the gas–liquid interaction parameter in relation (19) can be neglected. The critical capacity factor then can be written in

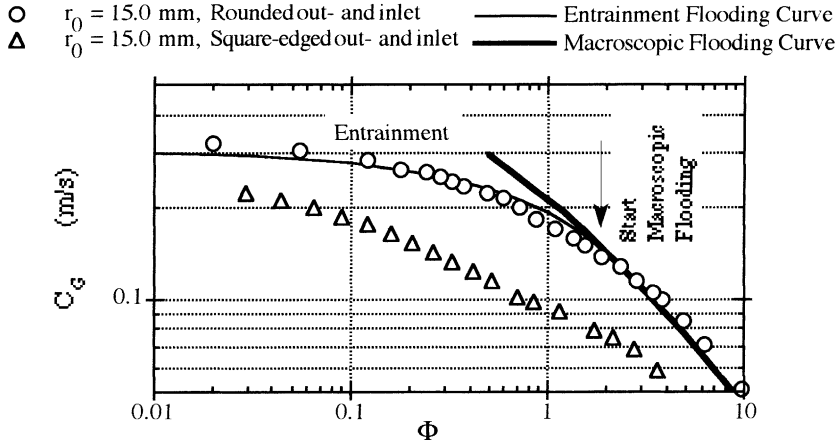

Fig. 5. The critical capacity factor as function of the flow parameter. The data points are measured by [7]. The thin line represents the curve calculated with Eq. (19), while the bold line indicates the macroscopic flood point due to frictional forces.

a more explicit form as

$$C_G^{crit}=1.135\,\theta^2\sqrt{g\,\theta r_0}\,Re_G^{1/32}\left(\frac{\sigma}{\theta^2 r_0^2 g(\rho_L-\rho_G)}\right)^{3/16}. \quad (20)$$

Here, use has been made of the Blasius friction factor for smooth pipes. The equation enables a direct comparison with existing explicit correlations, especially in regard to the influence of physical properties of the flows. When the equation is rewritten as a Kutateladze number (see [26]), it becomes close to the empirical relation given by [27] and modified by [11].

The above analysis once again shows the sensitivity of the flooding phenomenon. Its initiation in a vertical pipe is already influenced by the length of the pipe [6] and the in- and outlet conditions [7]. Due to the fact that flooding exhibits a large hysteresis [28], the subsequent theoretical difficulties even deteriorate. The hysteresis means that after the start of flooding one has to decrease the liquid or gas flows substantially to obtain de-flooding. Flooding, therefore, occurs over a wide flow range. A full theoretical description of flooding would require the prediction of both the flood point and the de-flood point. Although, it is already practice to measure both flood and de-flood point in vertical pipes, it is not yet common in packed bed studies.

5.2. Packed bed

Despite the theoretical difficulties, relation (18) contains much information on the behaviour of packed beds. This regards the geometrical packing characteristics and physical properties of the flow system. Fig. 6 shows the comparison of the calculated curves for several packing geometries with an effective inclination angle of 38° and the correlation of [29] for Mellapak 250Y.

The packing characteristics for the calculations are based on the Mellapak series of Sulzer. The used inclination angle is determined from dry pressure drop. Although, the shapes of the calculated curves are approximately identical for all packing sizes, the slopes of the measured and estimated curves are quite different. The measured critical capacity factor curve can be represented in analogy with Eq. (4) by:

$$C_{G,meas}^{crit}=C_r\frac{0.173}{(1+1.2\sqrt{\Phi})^2}, \quad (21)$$

while the critical capacity curve up to the macroscopic flooding area as calculated with the model can be correlated as

$$C_{G,model}^{crit}=C_r\frac{0.122}{(1+0.15\sqrt{\Phi})^2}. \quad (22)$$

The capacity of a different geometry is represented by the relative capacity factor C_r, which compares the packing with a well-studied geometry. In principle we can only speculate on the difference between the estimated curves and the measured curves, but it could be explained by the fact that in packed beds several locations in the geometry can cause a local increase of the liquid hold-up. These obstructions for the gas flow cause an increase of the gas velocity, pressure drop and liquid entrainment. Due to these disturbances the flooding phenomenon starts sooner than predicted with the model of Eq. (18), that is related to an undisturbed flow. This is similar to the much lower capacity of a vertical with square edge in- and outlet, as shown in Fig. 5. These theoretical difficulties cannot be solved in principle. However, when the disturbed capacity factor remains proportionally connected with the undisturbed capacity factor, a relative capacity factor (C_r) can be estimated via a comparison of the undisturbed capacity model. The relative capacity factor of a packing geometry with specific area, void fraction and effective inclination angle, applying a gas–liquid system can

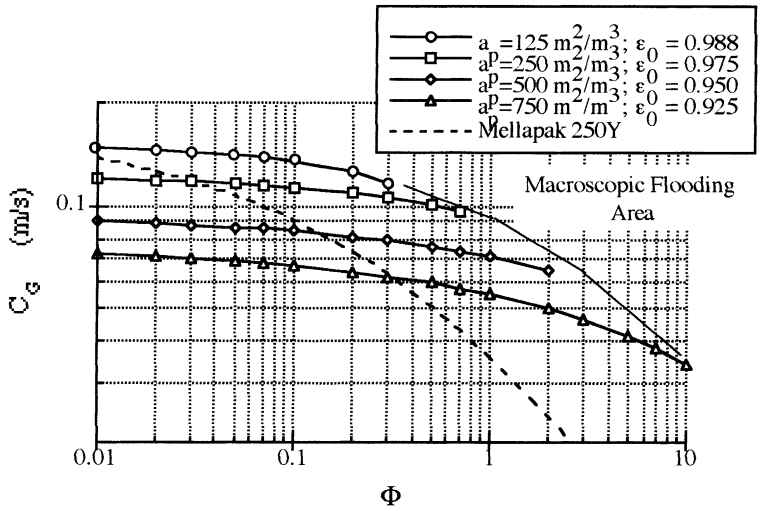

Fig. 6. The critical capacity factor as function of the flow factor for packing with an inclination angle of 38° calculated with the Eqs. (12) and (16) and the correlation given by [29].

Table 1
The estimated relative critical capacity factors for various packing sizes using Eqs. (18) and (23), compared with the data given by the supplier [28][a]

Type Mellapak	a_p (m^2/m^3)	ϵ_0 (m^3/m^3)	α (°)	C_r	$C_{r,model}$	ΔC (%)
125X	125	0.988	26	1.50	1.54	2.9
125Y	125	0.988	38	1.25	1.21	−3.1
170X	170	0.983	26	1.51	1.43	−5.2
170Y	170	0.983	38	1.14	1.12	−1.4
M2X	200	0.980	26	1.41	1.37	−3.1
M2Y	200	0.980	38	1.09	1.07	−1.6
250X	250	0.975	26	1.25	1.27	1.8
250Y	250	0.975	38	1.00	1.00	−0.4
350X	350	0.965	26	1.10	1.12	2.1
350Y	350	0.965	38	0.85	0.87	2.8
500X	500	0.950	26	1.00	0.96	−4.1
500Y	500	0.950	38	0.70	0.74	5.9
750Y	750	0.925	38	0.63	0.59	−5.9

[a] The estimated values are obtained using a water–air system in a column with a diameter of 0.5 m. Also indicated are the specific surface areas, void fractions and the effective inclination angle as determined from the pressure drop.

then be expressed as

$$C_r = \frac{C^{crit}_{G,meas}(type, \sigma, \rho_L, \rho_G, \eta_L, \eta_G)}{C^{crit}_{G,meas}(250Y, \sigma_{ref}, \rho_{L\text{-ref}}, \rho_{G\text{-ref}}, \eta_{L\text{-ref}}, \eta_{G\text{-ref}})} = \frac{C^{crit}_{G,model}(type, \sigma, \rho_L, , \rho_G, \eta_L, \eta_G)}{C^{crit}_{G,model}(250Y, \sigma_{ref}, \rho_{L\text{-ref}}, \rho_{G\text{-ref}}, \eta_{L\text{-ref}}, \eta_{G\text{-ref}})}. \quad (23)$$

In this study, Mellapak 250Y and the water–air system are used as a reference. Hypothesis (23) can be tested by comparing flooding data for different geometries and systems with other physical properties.

5.3. Geometrical influences on the flood point

Table 1 shows a comparison of the measured relative capacity factors, reported by [29] for the Mellapak series and the estimated relative capacity factors applying Eq. (18) in hypothesis (23). No substantial deviations from the reported values are found, so that hypothesis (23) appears valid. The principle should remain valid for random packing. Table 2 shows a list of random packing elements and their characteristic parameters [30]. The effective inclination angles are taken as 55° except for the raschig rings were an effective inclination angle of 65° was applied. The bold values in this table indicate macroscopic flooding.

The estimated relative capacity parameters for random packing show more deviations than those calculated for structured packing, but they still agree reasonably well with the measured values. When flooding is caused by the macroscopic mechanism one should double check the outcome of the critical capacity factor. Although, most random packings have similar effective inclination angles, it is not a general result. [31] for instance, increased the capacity for a packed column by a factor 2.3 using stacked rings. This means a reduction of the effective inclination angle by approximately 30°.

Table 2
Characteristic parameters of various types of random packing. Indicated are the element size, the void fraction and the specific area[a]

Size (mm)	ϵ_0 (m^3/m^3)	a_p (m^2/m^3)	C_r	$C_{r,model}$	ΔC_r (%)
Berl Saddles (ceramic)					
6	0.60	899	0.17	0.18	8
13	0.63	466	0.33	0.28	−14
19	0.66	269	0.39	0.40	1
25	0.69	249	0.49	0.44	−10
38	0.75	144	0.63	0.61	−4
50	0.72	105	0.76	0.68	−11
Raschig rings (metal)					
6	0.69	774	0.19	0.18	−7
13	0.84	420	0.29	0.33	13
19	0.88	274	0.41	0.43	6
25	0.92	206	0.48	0.52	9
Pall rings (metal)					
16	0.93	341	0.61	0.59	−3
25	0.94	206	0.74	0.75	3
38	0.95	128	0.96	0.90	−6
50	0.96	102	1.14	1.07	−6
Pall rings (plastic)					
16	0.87	341	0.52	0.53	2
25	0.90	206	0.71	0.69	−3
38	0.91	128	0.81	0.82	2
50	0.92	102	1.02	0.95	−7
89	0.92	85	1.27	1.00	−21

[a] The relative capacity parameter [30] is compared with the relative capacity parameter estimated with Eq. (23) at a flow parameter of 0.03. In these calculations use is made of an effective inclination angle of 55° and a column diameter of 0.5 m. For the Raschig ring an effective inclination angle of 65° is applied.

As mentioned before, flooding is influenced by a number of parameters and one that is often neglected is the influence of the column diameter. In the presented model the column diameter mainly affects the pressure drop and, therefore, the dissipated energy. As a consequence the dissipated energy will affect the maximum droplet size and, therefore, the flood point. Fig. 7 illustrates the influences on the flood point caused by the column diameter for structured and random packing. The change in capacity factor is compared with the relative capacity factor obtained for infinite column diameter ($C_{r,\infty}$). Although, the changes are not substantial, the figure again illustrates the dependence of the flood point for various parameters. The opposite effect of the column diameter on structured and random packing is caused by the decrease of the effective inclination angle for random packing with decreasing column diameter, so that the total pressure drop reduces, while for structured packing the pressure drop increases with decreasing column diameter (see also [2]).

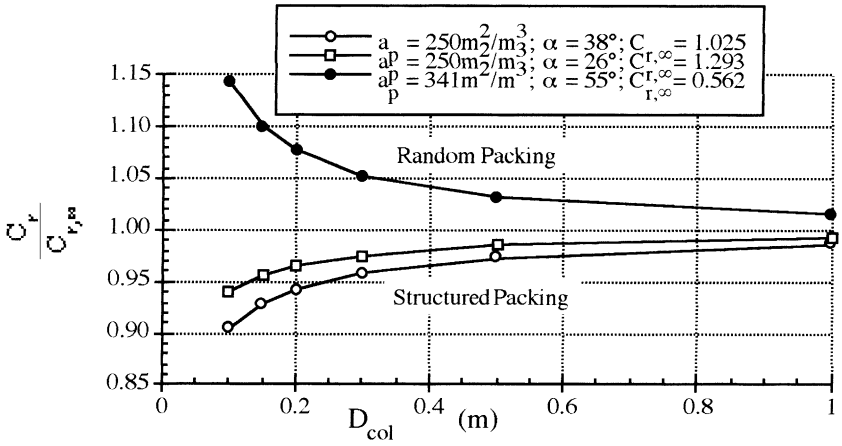

Fig. 7. The relative influence of the column diameter on the critical capacity factor for structured packing and random packing. The influence is obtained by comparing them with the indicated critical capacity factor at infinite column diameter.

6. Influence of physical properties on the flood point

In addition to the packing characteristics, the physical properties will influence the critical capacity factor. Since all properties are covered by Eq. (18), the described influence of the physical properties should agree with those found in literature, so that the prediction of the relative capacity factor as function of the physical properties is possible. In literature, these influences on the capacity are often described by applying a relative power function. The influence of the liquid viscosity and the surface tension on the relative capacity parameter is described using a correction (C_{cor}) factor as

$$C_{\mathrm{cor}} = \frac{C_{\mathrm{G}}^{\mathrm{crit}}(\sigma, \eta_{\mathrm{L}})}{C_{\mathrm{G}}^{\mathrm{crit}}(\sigma_{\mathrm{ref}}, \eta_{\mathrm{L\text{-}ref}})} = \frac{C_{\mathrm{G,model}}^{\mathrm{crit}}(\sigma, \eta_{\mathrm{L}})}{C_{\mathrm{G,model}}^{\mathrm{crit}}(\sigma_{\mathrm{ref}}, \eta_{\mathrm{L\text{-}ref}})} = C_{\mathrm{cor},\sigma} C_{\mathrm{cor},\eta_{\mathrm{L}}} = \left(\frac{\sigma}{\sigma_{\mathrm{ref}}}\right)^{m_1} \left(\frac{\eta_{\mathrm{L}}}{\eta_{\mathrm{L\text{-}ref}}}\right)^{m_2}, \qquad (24)$$

where m_1 and m_2 are constants. Eq. (24) is applied to compare known correlations for physical properties with the presented model. As in the present study, in most cases the ambient water–air system is taken as reference.

6.1. The surface tension

Eq. (20) shows that the surface tension influence on the critical capacity factor for a vertical pipe as $m_1 = 3/16 = 0.1875$. This value is well in agreement with the predicted dependencies using other theoretical consideration, which normally leads to a value of: $m_1 = 0.25$ (see, e.g. [12,22,32]) and published correlations ([11,27] $m_1 = 0.155$). For packed columns the reported influence of the surface tension on the critical capacity varies considerably. Most studies neglect the influence [29,31,33], but surface tension effects are reported by for instance [34], ($m_1 = 0.16$) and for liquid–liquid extraction by [35], $m_1 = 0.125$ and [9] ($m_1 = 0.20$). The results of the presented model are shown in Fig. 8. For comparison the estimated points are fitted using the power correlation (24). The figure shows that influence of the surface tension can be described reasonably well by using a power term. Interesting enough it also shows that the power coefficient depends on both the surface area and the inclination angle of the packing geometry. This effect was also observed by [36] for liquid–liquid extractions in randomly packed columns. When applying a large specific area for the application, the flood point is hardly influenced by the surface tension. Because of the large effective inclination angle, the surface tension influence on the critical capacity factor for random packing is limited. The calculations were carried out at a flow parameter of 0.03, but the choice of the flow parameter does not significantly affect the surface tension influence on the estimated capacity factor.

6.2. The liquid viscosity

The viscosity affects the critical capacity factor mainly through the square of the reduced hydraulic diameter (θ^2). This factor, describing the irrigation of the bed, reduces the total void fraction and, therefore, increases the gas velocity. Some reported power values for packed columns are: [29]: not reported; [37]: $m_2 = -0.05$; [31]: $m_2 = -0.1$; [34]: $m_2 = -0.11$; [32]: $m_2 = -0.17$. Fig. 9 shows the influence as estimated by our model over a wide viscosity range.

The normalised power term for the viscosity describes the influence not as well as the power function for the interfacial tension. This could explain the large deviations for the reported correlations. The viscosity in the presented model affects the critical capacity parameter in another way as well. In addition to the effect on the irrigation, an opposite influence on the capacity is caused by the interface velocity. A larger viscosity decreases the interface velocity and, therefore, reduces the pressure drop over the packing. The smaller pressure drop allows larger droplets the gas phase. This effect is most pronounced for packing with small

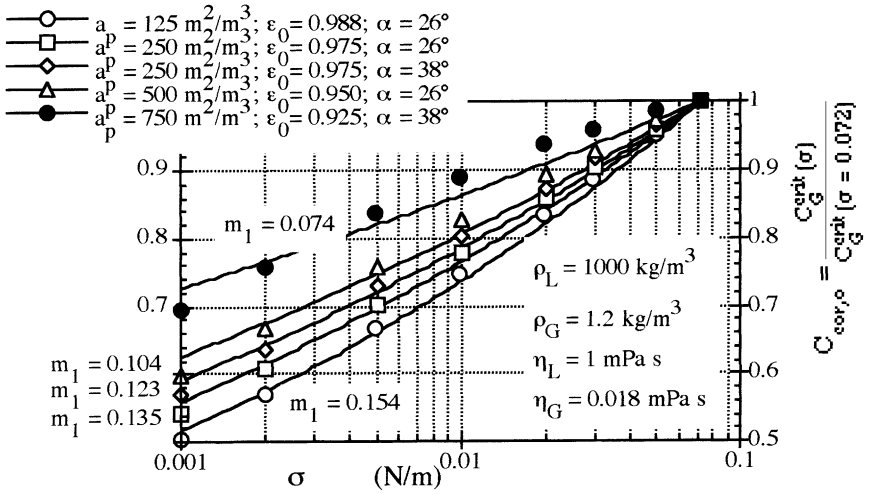

Fig. 8. The relative influence of the surface tension on the critical capacity factor for various types of packing for constant other physical properties as calculated with Eqs. (24) and (18). Indicated are the on the calculated data points fitted powers.

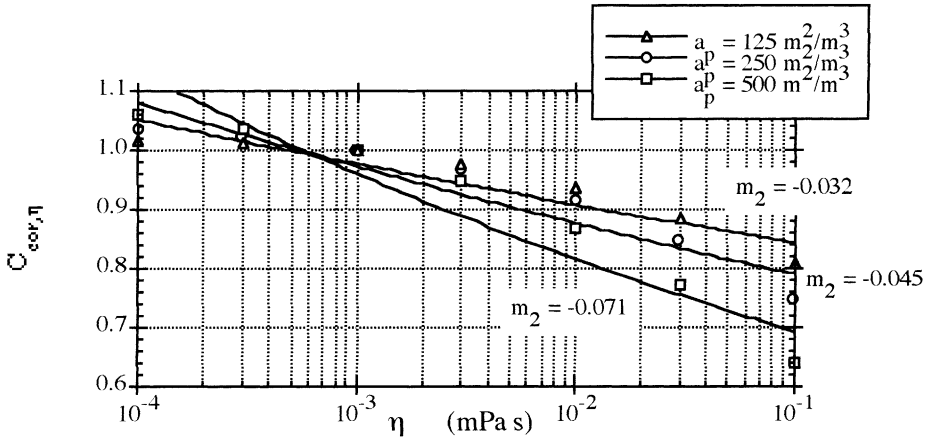

Fig. 9. The relative influence of the liquid viscosity on the capacity factor for three packing types with inclination angle of 38°. The indicated power terms are fitted on the calculated relative values of $C_{cor,\eta}$. The points are obtained at a flow parameter of 0.1.

specific area. The effective inclination angle hardly affects the viscosity influence, so that an estimated value for a packing with identical specific surface area, but different inclination angles, nearly coincide. The effect of the viscosity on the critical capacity factor is also shown in Fig. 10A and B. Fig. 10A shows the measured critical capacity factors, while the right graph shows the normalised critical capacity factors. Although, the surface tension also has some influence in this case, the differences are mainly caused by irrigated bed correction (θ^2).

6.3. The gas density

At elevated pressures one of the main considerations is the influence of the gas density on the capacity. Fig. 11A and B show the relative change of the critical capacity factor in comparison with a gas of density 1.2 kg/m^3 for two flow parameters. The figure shows that the gas density has a major influence on the critical capacity factor only for relative small specific area and effective inclination angle. The decrease of the curves at "low" gas density (<200 kg/m^3) is caused by the interface velocity. The interface velocity relatively increases towards the gas velocity when the gas density is increased.

The dissipated kinetic energy depends on the third power of the velocity, this parameter decreases at "large" gas densities, so that the maximum stable drop size and the critical gas velocity will increase. Only limited data are reported on the change of the flood point with increasing gas density. [38] measured pressure drops and flood points at high pressures for various random packing systems. They did not find any change of the critical capacity factor for pressures up to 100 bar in packed columns for ceramic Berl Saddles ($a_p = 386$, $\epsilon_0 = 0.59$) and for ceramic Raschig rings ($a_p = 309$, $\epsilon_0 = 0.68$). They used a methanol–nitrogen flow system. When the critical capacity factors are estimated using

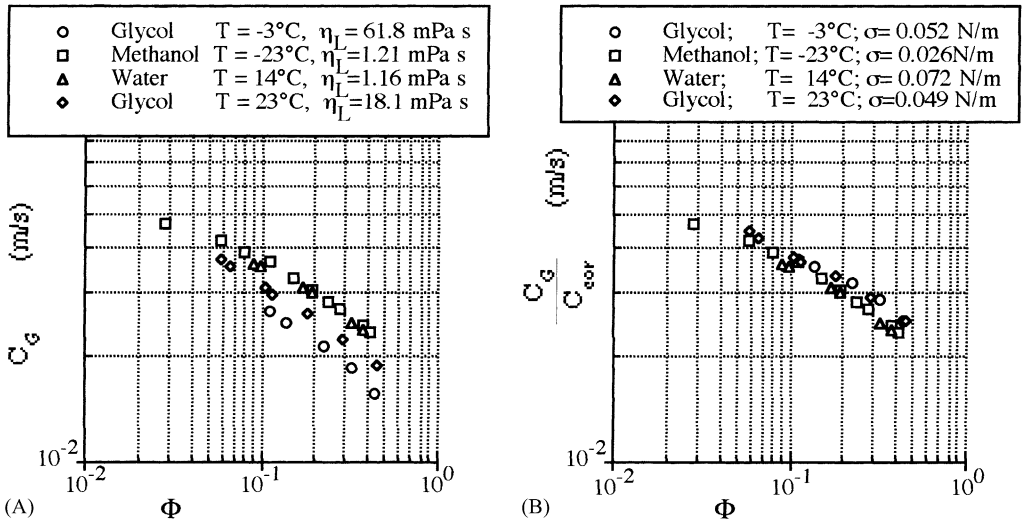

Fig. 10. (A) The measured critical capacity factors of ceramic Berl Saddles, ($a_p = 303 m^2/m^3$, $\epsilon_0 = 0.59$, $\alpha = 55$) as reported by [38]. (B) The corrected critical capacity factors of ceramic Berl Saddles, for various liquids with different viscosities and surface tensions as reported by [38].

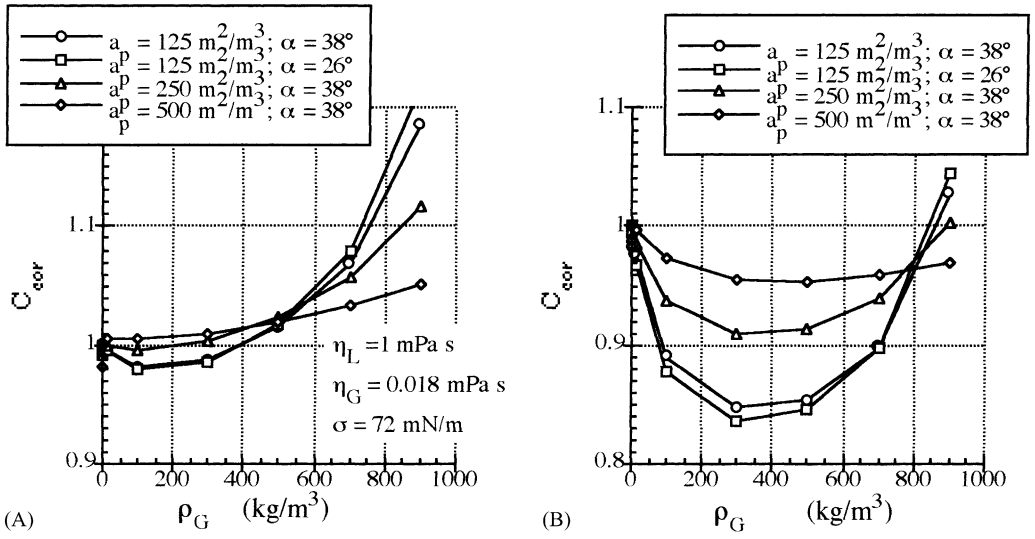

Fig. 11. (A) The relative influence of the gas density on the critical capacity factor for a series of structured packing at constant flow parameter ($\Phi = 0.01$). (B) The relative influence of the gas density on the critical capacity factor for a series of structured packing at constant flow parameter ($\Phi = 0.1$).

Eq. (18), a change of less than 1% is found over the applied density compared with the relative critical capacity factor for an ambient water–air system. The model, therefore, remains consistent with the reported results.

6.4. The gas viscosity

Since the flow of the gas is turbulent the influence of the gas viscosity in Eq. (18) is incorporated by making use of the smooth pipe friction factor. The relative effect of this parameter on the estimated critical capacity factor with constant other properties is limited and it seldom causes a change in the critical capacity factor over 5%.

Because in liquid–liquid contactors the flow is often laminar, an influence of the continuous phase viscosity is expected. If we use a laminar friction factor instead of the Blasius friction factor, the exponent of the "gaseous" Reynolds number in Eq. (20) increases form 1/32–1/8. Although, [39] report a dependence of the bulk phase viscosity as $(\eta_G/\eta_{G\text{-ref}})^{-0.33}$, it is identical with the dependence reported by [40], $(\eta_G/\eta_{G\text{-ref}})^{-0.125}$. However, most correlation do not include a bulk phase viscosity [9], for $Re_G > 50$, [35,36].

7. Concluding remarks

The presented model provides an estimation method that describes the relative changes of flood point with the physical properties and geometry of the packing. This has been

accomplished by taking into account the lift force: $F_1 \sim d_e^3 \rho_G u_G(r)\,(\partial u_G(r)/\partial r)$, on entrained droplet. Using this additional force, it is possible to predict several observed phenomenon concerning physical properties and geometry of the packing. More elaborate descriptions concerning all influences on a droplet in a velocity field, distinguish even more forces on the droplet (see, e.g. [41]. However, most of these forces include a gas velocity and a gas velocity gradient and can be written similar to the expression used. It, therefore, appears justified to conclude that the presented description provides a more fundamental basis for the flooding phenomenon than correlations reported earlier and consequently predicts several of the observed flooding phenomenon.

The presented model predicts and explains some of phenomenon concerning flooding. However, it does not explain the total flooding phenomenon. As is shown in this study, this total explanation cannot be expected from any theory. However, by comparing two undisturbed capacity factors a relative capacity factor can be estimated provided that the disturbed capacity factor remains proportionally connected with the undisturbed capacity factor. This is a necessary "calibration" with a well-known geometry. The dependence of the critical capacity factor on subtle factors as the pipe length and a smooth gas and liquid entrance [7,11] in a vertical pipe geometry strengthens the concept of calibration. Experimentally, it is necessary to research the hysteresis of the flooding phenomenon. It is likely that the de-flood mechanism is a less sensitive phenomenon, so that it can be used as lower limit for flooding.

References

[1] B.E.T. Hutton, L.S. Leung, P.C. Brooks, D.J. Nicklin, On flooding in packed columns, Chem. Eng. Sci. 29 (1974) 493–500.

[2] G.F. Woerlee, J. Berends, Z. Olujic, J. de Graauw, A Comprehensive Model for the Pressure Drop in Packed Columns, 1999, submitted for publication.

[3] V. Kaiser, Flooding in Packed Columns Correlated Another Way, AIChE Spring National Meeting, March/April 1993, Houston (see also Chem. Eng. Progr. 90 (6) (1994) 55–59).

[4] P.B. Whalley, Two-Phase Flow and Heat Transfer, Oxford University Press, Oxford, 1996.

[5] G.F. Hewitt, G.B. Wallis, Flooding and Associated Phenomena in Falling Film Flow in a Tube, UKAERE Report, R-4022 (1963).

[6] A.H. Govan, G.F. Hewitt, H.J. Richter, A. Scott, Flooding and churn flow in vertical pipes, Int. J. Multiphase Flow 17 (1) (1990) 27–44.

[7] J.H. Jeong, H.C. No, Experimental study of the effect of pipe length and pipe-end geometry on flooding, Int. J. Multiphase Flow 22 (1996) 499–514.

[8] G.B. Wallis, One-Dimensional Two-Phase Flow, McGraw-Hill, New York, 1969.

[9] J.W. Crawford, C.R. Wilke, Limiting flows in packed extraction columns, Chem. Eng. Progr. 47 (8) (1951) 423–431.

[10] G.S. Laddha, T.E. Degaleesan, Transport Phenomena in Liquid Extraction, McGraw-Hill, New Delhi, 1976.

[11] K.W. McQuillan, P.B. Whalley, A comparison between flooding and experimental flooding data for gas–liquid flow in vertical circular tubes, Chem. Eng. Sci. 40 (1984) 1425–1440.

[12] M. Ishii, M.A. Grolmes, Inception criteria for droplet entrainment in two-phase concurrent film flow, AIChE J. 21 (1975) 308–317.

[13] G.F. Hewitt, N.S. Hall-Taylor, Annular Two-Phase Flow, Pergamon Press, New York, 1970.

[14] J.R. Fair, J.L. Bravo, Distillation columns containing structured packing, Chem. Eng. Progr. 86 (1990) 19–29.

[15] R.H. Sabersky, A.J. Acosta, E.G. Hauptmann, Fluid Flow, 3rd Edition, MacMillan, New York, 1989.

[16] R.P. Feynman, R.B. Leighton, M. Sands, Lectures on Physics, Addison-Wesley, Reading, MA, 1963.

[17] L. Rayleigh, On the instability of jets, Proc. Lond. Math. Soc. 10 (1878) 4–13.

[18] R. Clift, J.R. Grace, M.E. Weber, Bubbles, Drops, and Particles, Academic Press, New York, 1978.

[19] R. Datta, Eddy viscosity and velocity distribution in turbulent pipe flow revisited, AIChE J. 39 (7) (1993) 1107–1112.

[20] J.M. Coulson, J.F. Richardson, Chemical Engineering, Vol. 2, 3rd Edition, Pergamon Press, Oxford, 1978.

[21] J.O. Hinze, Fundamentals of the hydrodynamic mechanism of splitting in dispersion processes, AIChE J. 1 (1954) 289–295.

[22] Y. Taitel, D. Barnea, A.E. Dukler, Modelling flow pattern transitions for steady upward gas–liquid flow in vertical tubes, AIChE J. 26 (3) (1980) 345.

[23] J.O. Hinze, Turbulence, 2nd Edition, McGraw-Hill, New York, 1975.

[24] D.C. Batchelor, Proc. Cambridge Phil. Soc. 47 (1951) 359.

[25] M.H.I. Baird, S.J. Lane, Drop size and hold-up in a reciprocating plate extraction column, Chem. Eng. Sci. 28 (1972) 947–957.

[26] O.L. Pushkina, Y.L. Sorokin, Breakdown of liquid film motion in vertical tubes, Heat Transfer Soviet Res. 1 (1969) 56–64.

[27] V.P. Alekseev, A.E. Poberezkin, P.V. Gerasimov, Determination of flooding rates in regular packing, Heat Transfer Soviet Res. 4 (1972) 159–163.

[28] G.P. Celata, M. Cumo, G.E. Farello, T. Setaro, Hysteresis effect in flooding, Int. J. Multiphase Flow 17 (2) (1991) 283–289.

[29] Sulzer Brother Ltd., Separation Columns for Distillation and Absorption, Information Bulletin, 1989.

[30] R.E. Treybal, Mass Transfer Operations, 3rd Edition, Series in Chemical Engineering, Wiley, New York, 1980.

[31] T.K. Sherwood, G.H. Schipley, F.A. Holloway, Flooding velocity in packed columns, Ind. Eng. Chem. 30 (1938) 765–769.

[32] G.B. Wallis, Flooding Velocities for Air and Water in Vertical Tubes, Report AEEW-R123 (1961).

[33] A. Mersmann, Zur Berechnung des Flutpunktes in Füllkörperschüttungen, Chem. Ing. Techn. 37 (3) (1965) 218–226.

[34] Norton Chemical Process Products Corporation, Intalox High-Performance Structured Packing, Information Bulletin, 1993.

[35] F.R. Dell, H.R.C. Pratt, Symposium on liquid–liquid extraction, part I. Flooding rates for packed columns, Trans. Inst. Chem. Eng. 29 (1951) 89.

[36] G. Venkataraman, G.S. Laddha, AIChE J. 6 (1960) 355.

[37] J.M. Coulson, J.F. Richardson, Chemical Engineering (Design), Vol. 6, Pergamon Press, Oxford, 1985.

[38] H. Krehenwinkel, H. Knapp, Pressure drop and flooding in packed columns operating at high pressures, Chem. Eng. Tech. 10 (1987) 231–242.

[39] R.R. Breckenfeld, C.R. Wilke, Chem. Eng. Progr. 46 (1950) 187.

[40] E.H. Hoffing, F.J. Lockhart, A correlation of flooding velocities in packed columns, Chem. Eng. Progr. 50 (1954) 94–103.

[41] C.W.M. Geld, Measurement and prediction of solid sphere trajectories in accelerated gas flow, Int. J. Multiphase Flow 23 (1997) 357–376.